Observation of $\eta_c(2S) \to 3(\pi^+\pi^-)$ and measurements of $\chi_{cJ} \to 3(\pi^+\pi^-)$ in $\psi(3686)$ radiative transitions

M. Ablikim,[1] M. N. Achasov,[11,b] P. Adlarson,[70] M. Albrecht,[4] R. Aliberti,[31] A. Amoroso,[69a,69c] M. R. An,[35] Q. An,[66,53] X. H. Bai,[61] Y. Bai,[52] O. Bakina,[32] R. Baldini Ferroli,[26a] I. Balossino,[1,27a] Y. Ban,[42,g] V. Batozskaya,[1,40] D. Becker,[31] K. Begzsuren,[29] N. Berger,[31] M. Bertani,[26a] D. Bettoni,[27a] F. Bianchi,[69a,69c] J. Bloms,[63] A. Bortone,[69a,69c] I. Boyko,[32] R. A. Briere,[5] A. Brueggemann,[63] H. Cai,[71] X. Cai,[1,53] A. Calcaterra,[26a] G. F. Cao,[1,58] N. Cao,[1,58] S. A. Cetin,[57a] J. F. Chang,[1,53] W. L. Chang,[1,58] G. Chelkov,[32,a] C. Chen,[39] Chao Chen,[50] G. Chen,[1] H. S. Chen,[1,58] M. L. Chen,[1,53] S. J. Chen,[38] S. M. Chen,[56] T. Chen,[1] X. R. Chen,[28,58] X. T. Chen,[1] Y. B. Chen,[1,53] Z. J. Chen,[23,h] W. S. Cheng,[69c] S. K. Choi,[50] X. Chu,[39] G. Cibinetto,[27a] F. Cossio,[69c] J. J. Cui,[45] H. L. Dai,[1,53] J. P. Dai,[73] A. Dbeyssi,[17] R. E. de Boer,[4] D. Dedovich,[32] Z. Y. Deng,[1] A. Denig,[31] I. Denysenko,[32] M. Destefanis,[69a,69c] F. De Mori,[69a,69c] Y. Ding,[36] J. Dong,[1,53] L. Y. Dong,[1,58] M. Y. Dong,[1,53,58] X. Dong,[71] S. X. Du,[75] P. Egorov,[32,a] Y. L. Fan,[71] J. Fang,[1,53] S. S. Fang,[1,58] W. X. Fang,[1] Y. Fang,[1] R. Farinelli,[27a] L. Fava,[69b,69c] F. Feldbauer,[4] G. Felici,[26a] C. Q. Feng,[66,53] J. H. Feng,[54] K. Fischer,[64] M. Fritsch,[4] C. Fritzsch,[63] C. D. Fu,[1] H. Gao,[58] Y. N. Gao,[42,g] Yang Gao,[66,53] S. Garbolino,[69c] I. Garzia,[27a,27b] P. T. Ge,[71] Z. W. Ge,[38] C. Geng,[54] E. M. Gersabeck,[62] A. Gilman,[64] K. Goetzen,[12] L. Gong,[36] W. X. Gong,[1,53] W. Gradl,[31] M. Greco,[69a,69c] L. M. Gu,[38] M. H. Gu,[1,53] Y. T. Gu,[14] C. Y. Guan,[1,58] A. Q. Guo,[28,58] L. B. Guo,[37] R. P. Guo,[44] Y. P. Guo,[10,f] A. Guskov,[32,a] T. T. Han,[45] W. Y. Han,[35] X. Q. Hao,[18] F. A. Harris,[60] K. K. He,[50] K. L. He,[1,58] F. H. Heinsius,[4] C. H. Heinz,[31] Y. K. Heng,[1,53,58] C. Herold,[55] M. Himmelreich,[31,d] G. Y. Hou,[1,58] Y. R. Hou,[58] Z. L. Hou,[1] H. M. Hu,[1,58] J. F. Hu,[51,i] T. Hu,[1,53,58] Y. Hu,[1] G. S. Huang,[66,53] K. X. Huang,[54] L. Q. Huang,[67] L. Q. Huang,[28,58] X. T. Huang,[45] Y. P. Huang,[1] Z. Huang,[42,g] T. Hussain,[68] N. Hüsken,[25,31] W. Imoehl,[25] M. Irshad,[66,53] J. Jackson,[25] S. Jaeger,[4] S. Janchiv,[29] E. Jang,[50] J. H. Jeong,[50] Q. Ji,[1] Q. P. Ji,[18] X. B. Ji,[1,58] X. L. Ji,[1,53] Y. Y. Ji,[45] Z. K. Jia,[66,53] H. B. Jiang,[45] S. S. Jiang,[35] X. S. Jiang,[1,53,58] Y. Jiang,[58] J. B. Jiao,[45] Z. Jiao,[21] S. Jin,[38] Y. Jin,[61] M. Q. Jing,[1,58] T. Johansson,[70] N. Kalantar-Nayestanaki,[59] X. S. Kang,[36] R. Kappert,[59] M. Kavatsyuk,[59] B. C. Ke,[75] I. K. Keshk,[4] A. Khoukaz,[63] P. Kiese,[31] R. Kiuchi,[1] R. Kliemt,[12] L. Koch,[33] O. B. Kolcu,[57a] B. Kopf,[4] M. Kuemmel,[4] M. Kuessner,[4] A. Kupsc,[40,70] W. Kühn,[33] J. J. Lane,[62] J. S. Lange,[33] P. Larin,[17] A. Lavania,[24] L. Lavezzi,[69a,69c] Z. H. Lei,[66,53] H. Leithoff,[31] M. Lellmann,[31] T. Lenz,[31] C. Li,[43] C. Li,[39] C. H. Li,[35] Cheng Li,[66,53] D. M. Li,[75] F. Li,[1,53] G. Li,[1] H. Li,[47] H. Li,[66,53] H. B. Li,[1,58] H. J. Li,[18] H. N. Li,[51,i] J. Q. Li,[4] J. S. Li,[54] J. W. Li,[45] Ke Li,[1] L. J. Li,[1] L. K. Li,[1] Lei Li,[3] M. H. Li,[39] P. R. Li,[34,j,k] S. X. Li,[10] S. Y. Li,[56] T. Li,[45] W. D. Li,[1,58] W. G. Li,[1] X. H. Li,[66,53] X. L. Li,[45] Xiaoyu Li,[1,58] H. Liang,[66,53] H. Liang,[1,58] H. Liang,[30] Y. F. Liang,[49] Y. T. Liang,[28,58] G. R. Liao,[13] L. Z. Liao,[45] J. Libby,[24] A. Limphirat,[55] C. X. Lin,[54] D. X. Lin,[28,58] T. Lin,[1] B. J. Liu,[1] C. X. Liu,[1] D. Liu,[17,66] F. H. Liu,[48] Fang Liu,[1] Feng Liu,[6] G. M. Liu,[51,i] H. Liu,[34,j,k] H. B. Liu,[14] H. M. Liu,[1,58] Huanhuan Liu,[1] Huihui Liu,[19] J. B. Liu,[66,53] J. L. Liu,[67] J. Y. Liu,[1,58] K. Liu,[1] K. Y. Liu,[36] Ke Liu,[20] L. Liu,[66,53] Lu Liu,[39] M. H. Liu,[10,f] P. L. Liu,[1] Q. Liu,[58] S. B. Liu,[66,53] T. Liu,[10,f] W. K. Liu,[39] W. M. Liu,[66,53] X. Liu,[34,j,k] Y. Liu,[34,j,k] Y. B. Liu,[39] Z. A. Liu,[1,53,58] Z. Q. Liu,[45] X. C. Lou,[1,53,58] F. X. Lu,[54] H. J. Lu,[21] J. G. Lu,[1,53] X. L. Lu,[1] Y. Lu,[7] Y. P. Lu,[1,53] Z. H. Lu,[1] C. L. Luo,[37] M. X. Luo,[74] T. Luo,[10,f] X. L. Luo,[1,53] X. R. Lyu,[58] Y. F. Lyu,[39] F. C. Ma,[36] H. L. Ma,[1] L. L. Ma,[45] M. M. Ma,[1,58] Q. M. Ma,[1] R. Q. Ma,[1,58] R. T. Ma,[58] X. Y. Ma,[1,53] Y. Ma,[42,g] F. E. Maas,[17] M. Maggiora,[69a,69c] S. Maldaner,[4] S. Malde,[64] Q. A. Malik,[68] A. Mangoni,[26b] Y. J. Mao,[42,g,g] Z. P. Mao,[1] S. Marcello,[69a,69c] Z. X. Meng,[61] J. G. Messchendorp,[59,12] G. Mezzadri,[1,27a] H. Miao,[1] T. J. Min,[38] R. E. Mitchell,[25] X. H. Mo,[1,53,58] N. Yu. Muchnoi,[11,b] Y. Nefedov,[32] F. Nerling,[17,d] I. B. Nikolaev,[11] Z. Ning,[1,53] S. Nisar,[9,l] Y. Niu,[45] S. L. Olsen,[58] Q. Ouyang,[1,53,58] S. Pacetti,[26b,26c] X. Pan,[10,f] Y. Pan,[52] A. Pathak,[1] A. Pathak,[30] M. Pelizaeus,[4] H. P. Peng,[66,53] K. Peters,[12,d] J. Pettersson,[70] J. L. Ping,[37] R. G. Ping,[1,58] S. Plura,[31] S. Pogodin,[32] V. Prasad,[66,53] F. Z. Qi,[1] H. Qi,[66,53] H. R. Qi,[56] M. Qi,[38] T. Y. Qi,[10,f] S. Qian,[1,53] W. B. Qian,[58] Z. Qian,[54] C. F. Qiao,[58] J. J. Qin,[67] L. Q. Qin,[13] X. P. Qin,[10,f] X. S. Qin,[45] Z. H. Qin,[1,53] J. F. Qiu,[1] S. Q. Qu,[39] S. Q. Qu,[56] K. H. Rashid,[68] C. F. Redmer,[31] K. J. Ren,[35] A. Rivetti,[69c] V. Rodin,[59] M. Rolo,[69c] G. Rong,[1,58] Ch. Rosner,[17] S. N. Ruan,[39] H. S. Sang,[66] A. Sarantsev,[32,c] Y. Schelhaas,[31] C. Schnier,[4] K. Schönning,[70] M. Scodeggio,[27a,27b] K. Y. Shan,[10,f] W. Shan,[22] X. Y. Shan,[66,53] J. F. Shangguan,[50] L. G. Shao,[1,58] M. Shao,[66,53] C. P. Shen,[10,f] H. F. Shen,[1,58] X. Y. Shen,[1,58] B. A. Shi,[58] H. C. Shi,[66,53] J. Y. Shi,[1] Q. Q. Shi,[50] R. S. Shi,[1,58] X. Shi,[1,53] X. D. Shi,[66,53] J. J. Song,[18] W. M. Song,[1,30] Y. X. Song,[42,g] S. Sosio,[69a,69c] S. Spataro,[69a,69c] F. Stieler,[31] K. X. Su,[71] P. P. Su,[50] Y. J. Su,[58] G. X. Sun,[1] H. Sun,[58] H. K. Sun,[1] J. F. Sun,[18] L. Sun,[71] S. S. Sun,[1,58] T. Sun,[1,58] W. Y. Sun,[30] X. Sun,[23,h] Y. J. Sun,[66,53] Y. Z. Sun,[1] Z. T. Sun,[45] Y. H. Tan,[71] Y. X. Tan,[66,53] C. J. Tang,[49] G. Y. Tang,[1] J. Tang,[54] L. Y. Tao,[67] Q. T. Tao,[23,h] M. Tat,[64] J. X. Teng,[66,53] V. Thoren,[70] W. H. Tian,[47] Y. Tian,[28,58] I. Uman,[57b] B. Wang,[1] B. L. Wang,[58] C. W. Wang,[38] D. Y. Wang,[42,g] F. Wang,[67] H. J. Wang,[34,j,k] H. P. Wang,[1,58] K. Wang,[1,53] L. L. Wang,[1] M. Wang,[45] M. Z. Wang,[42,g] Meng Wang,[1,58] S. Wang,[13] S. Wang,[10,f] T. Wang,[10,f] T. J. Wang,[39] W. Wang,[54] W. H. Wang,[71] W. P. Wang,[66,53] X. Wang,[42,g] X. F. Wang,[34,j,k] X. L. Wang,[10,f] Y. D. Wang,[41] Y. F. Wang,[1,53,58] Y. H. Wang,[43] Y. Q. Wang,[1] Yaqian Wang,[1,16] Yi Wang,[56] Z. Wang,[1,53] Z. Y. Wang,[1,58] Ziyi Wang,[58] D. H. Wei,[13] F. Weidner,[63] S. P. Wen,[1] D. J. White,[62] U. Wiedner,[4] G. Wilkinson,[64] M. Wolke,[70] L. Wollenberg,[4] J. F. Wu,[1,58] L. H. Wu,[1] L. J. Wu,[1,58] X. Wu,[10,f] X. H. Wu,[30] Y. Wu,[66] Z. Wu,[1,53] L. Xia,[66,53] T. Xiang,[42,g] D. Xiao,[34,j,k] G. Y. Xiao,[38] H. Xiao,[10,f] S. Y. Xiao,[1] Y. L. Xiao,[10,f] Z. J. Xiao,[37]

C. Xie,[38] X. H. Xie,[42,g] Y. Xie,[45] Y. G. Xie,[1,53] Y. H. Xie,[6] Z. P. Xie,[66,53] T. Y. Xing,[1,58] C. F. Xu,[1] C. J. Xu,[54] G. F. Xu,[1] H. Y. Xu,[61] Q. J. Xu,[15] X. P. Xu,[50] Y. C. Xu,[58] Z. P. Xu,[38] F. Yan,[10,f] L. Yan,[10,f] W. B. Yan,[66,53] W. C. Yan,[75] H. J. Yang,[46,e] H. L. Yang,[30] H. X. Yang,[1] L. Yang,[47] S. L. Yang,[58] Tao Yang,[1] Y. F. Yang,[39] Y. X. Yang,[1,58] Yifan Yang,[1,58] M. Ye,[1,53] M. H. Ye,[8] J. H. Yin,[1] Z. Y. You,[54] B. X. Yu,[1,53,58] C. X. Yu,[39] G. Yu,[1,58] T. Yu,[67] X. D. Yu,[42,g] C. Z. Yuan,[1,58] L. Yuan,[2] S. C. Yuan,[1] X. Q. Yuan,[1] Y. Yuan,[1,58] Z. Y. Yuan,[54] C. X. Yue,[35] A. A. Zafar,[68] F. R. Zeng,[45] X. Zeng,[6] Y. Zeng,[23,h] Y. H. Zhan,[54] A. Q. Zhang,[1] B. L. Zhang,[1] B. X. Zhang,[1] D. H. Zhang,[39] G. Y. Zhang,[18] H. Zhang,[66] H. H. Zhang,[54] H. H. Zhang,[30] H. Y. Zhang,[1,53] J. L. Zhang,[72] J. Q. Zhang,[37] J. W. Zhang,[1,53,58] J. X. Zhang,[34,j,k] J. Y. Zhang,[1] J. Z. Zhang,[1,58] Jianyu Zhang,[1,58] Jiawei Zhang,[1,58] L. M. Zhang,[56] L. Q. Zhang,[54] Lei Zhang,[38] P. Zhang,[1] Q. Y. Zhang,[35,75] Shuihan Zhang,[1,58] Shulei Zhang,[23,h] X. D. Zhang,[41] X. M. Zhang,[1] X. Y. Zhang,[45] X. Y. Zhang,[50] Y. Zhang,[64] Y. T. Zhang,[75] Y. H. Zhang,[1,53] Yan Zhang,[66,53] Yao Zhang,[1] Z. H. Zhang,[1] Z. Y. Zhang,[71] Z. Y. Zhang,[39] G. Zhao,[1] J. Zhao,[35] J. Y. Zhao,[1,58] J. Z. Zhao,[1,53] Lei Zhao,[66,53] Ling Zhao,[1] M. G. Zhao,[39] Q. Zhao,[1] S. J. Zhao,[75] Y. B. Zhao,[1,53] Y. X. Zhao,[28,58] Z. G. Zhao,[66,53] A. Zhemchugov,[32,a] B. Zheng,[67] J. P. Zheng,[1,53] Y. H. Zheng,[58] B. Zhong,[37] C. Zhong,[67] X. Zhong,[54] H. Zhou,[45] L. P. Zhou,[1,58] X. Zhou,[71] X. K. Zhou,[58] X. R. Zhou,[66,53] X. Y. Zhou,[35] Y. Z. Zhou,[10,f] J. Zhu,[39] K. Zhu,[1] K. J. Zhu,[1,53,58] L. X. Zhu,[58] S. H. Zhu,[65] S. Q. Zhu,[38] T. J. Zhu,[72] W. J. Zhu,[10,f] Y. C. Zhu,[66,53] Z. A. Zhu,[1,58] B. S. Zou,[1] and J. H. Zou[1]

(BESIII Collaboration)

[1]*Institute of High Energy Physics, Beijing 100049, People's Republic of China*
[2]*Beihang University, Beijing 100191, People's Republic of China*
[3]*Beijing Institute of Petrochemical Technology, Beijing 102617, People's Republic of China*
[4]*Bochum Ruhr-University, D-44780 Bochum, Germany*
[5]*Carnegie Mellon University, Pittsburgh, Pennsylvania 15213, USA*
[6]*Central China Normal University, Wuhan 430079, People's Republic of China*
[7]*Central South University, Changsha 410083, People's Republic of China*
[8]*China Center of Advanced Science and Technology, Beijing 100190, People's Republic of China*
[9]*COMSATS University Islamabad, Lahore Campus, Defence Road, Off Raiwind Road, 54000 Lahore, Pakistan*
[10]*Fudan University, Shanghai 200433, People's Republic of China*
[11]*G.I. Budker Institute of Nuclear Physics SB RAS (BINP), Novosibirsk 630090, Russia*
[12]*GSI Helmholtzcentre for Heavy Ion Research GmbH, D-64291 Darmstadt, Germany*
[13]*Guangxi Normal University, Guilin 541004, People's Republic of China*
[14]*Guangxi University, Nanning 530004, People's Republic of China*
[15]*Hangzhou Normal University, Hangzhou 310036, People's Republic of China*
[16]*Hebei University, Baoding 071002, People's Republic of China*
[17]*Helmholtz Institute Mainz, Staudinger Weg 18, D-55099 Mainz, Germany*
[18]*Henan Normal University, Xinxiang 453007, People's Republic of China*
[19]*Henan University of Science and Technology, Luoyang 471003, People's Republic of China*
[20]*Henan University of Technology, Zhengzhou 450001, People's Republic of China*
[21]*Huangshan College, Huangshan 245000, People's Republic of China*
[22]*Hunan Normal University, Changsha 410081, People's Republic of China*
[23]*Hunan University, Changsha 410082, People's Republic of China*
[24]*Indian Institute of Technology Madras, Chennai 600036, India*
[25]*Indiana University, Bloomington, Indiana 47405, USA*
[26a]*INFN Laboratori Nazionali di Frascati, I-00044 Frascati, Italy*
[26b]*INFN Sezione di Perugia, I-06100 Perugia, Italy*
[26c]*University of Perugia, I-06100 Perugia, Italy*
[27a]*INFN Sezione di Ferrara, I-44122 Ferrara, Italy*
[27b]*University of Ferrara, I-44122 Ferrara, Italy*
[28]*Institute of Modern Physics, Lanzhou 730000, People's Republic of China*
[29]*Institute of Physics and Technology, Peace Avenue 54B, Ulaanbaatar 13330, Mongolia*
[30]*Jilin University, Changchun 130012, People's Republic of China*
[31]*Johannes Gutenberg University of Mainz, Johann-Joachim-Becher-Weg 45, D-55099 Mainz, Germany*
[32]*Joint Institute for Nuclear Research, 141980 Dubna, Moscow region, Russia*
[33]*Justus-Liebig-Universitaet Giessen, II. Physikalisches Institut, Heinrich-Buff-Ring 16, D-35392 Giessen, Germany*
[34]*Lanzhou University, Lanzhou 730000, People's Republic of China*
[35]*Liaoning Normal University, Dalian 116029, People's Republic of China*
[36]*Liaoning University, Shenyang 110036, People's Republic of China*
[37]*Nanjing Normal University, Nanjing 210023, People's Republic of China*
[38]*Nanjing University, Nanjing 210093, People's Republic of China*
[39]*Nankai University, Tianjin 300071, People's Republic of China*
[40]*National Centre for Nuclear Research, Warsaw 02-093, Poland*

[41]*North China Electric Power University, Beijing 102206, People's Republic of China*
[42]*Peking University, Beijing 100871, People's Republic of China*
[43]*Qufu Normal University, Qufu 273165, People's Republic of China*
[44]*Shandong Normal University, Jinan 250014, People's Republic of China*
[45]*Shandong University, Jinan 250100, People's Republic of China*
[46]*Shanghai Jiao Tong University, Shanghai 200240, People's Republic of China*
[47]*Shanxi Normal University, Linfen 041004, People's Republic of China*
[48]*Shanxi University, Taiyuan 030006, People's Republic of China*
[49]*Sichuan University, Chengdu 610064, People's Republic of China*
[50]*Soochow University, Suzhou 215006, People's Republic of China*
[51]*South China Normal University, Guangzhou 510006, People's Republic of China*
[52]*Southeast University, Nanjing 211100, People's Republic of China*
[53]*State Key Laboratory of Particle Detection and Electronics, Beijing 100049, Hefei 230026, People's Republic of China*
[54]*Sun Yat-Sen University, Guangzhou 510275, People's Republic of China*
[55]*Suranaree University of Technology, University Avenue 111, Nakhon Ratchasima 30000, Thailand*
[56]*Tsinghua University, Beijing 100084, People's Republic of China*
[57a]*Turkish Accelerator Center Particle Factory Group, Istinye University, 34010, Istanbul, Turkey*
[57b]*Near East University, Nicosia, North Cyprus, Mersin 10, Turkey*
[58]*University of Chinese Academy of Sciences, Beijing 100049, People's Republic of China*
[59]*University of Groningen, NL-9747 AA Groningen, The Netherlands*
[60]*University of Hawaii, Honolulu, Hawaii 96822, USA*
[61]*University of Jinan, Jinan 250022, People's Republic of China*
[62]*University of Manchester, Oxford Road, Manchester M13 9PL, United Kingdom*
[63]*University of Muenster, Wilhelm-Klemm-Strasse 9, 48149 Muenster, Germany*
[64]*University of Oxford, Keble Road, Oxford OX13RH, United Kingdom*
[65]*University of Science and Technology Liaoning, Anshan 114051, People's Republic of China*
[66]*University of Science and Technology of China, Hefei 230026, People's Republic of China*
[67]*University of South China, Hengyang 421001, People's Republic of China*
[68]*University of the Punjab, Lahore-54590, Pakistan*
[69a]*University of Turin and INFN, University of Turin, I-10125 Turin, Italy*
[69b]*University of Eastern Piedmont, I-15121 Alessandria, Italy*
[69c]*INFN, I-10125 Turin, Italy*
[70]*Uppsala University, Box 516, SE-75120 Uppsala, Sweden*
[71]*Wuhan University, Wuhan 430072, People's Republic of China*
[72]*Xinyang Normal University, Xinyang 464000, People's Republic of China*
[73]*Yunnan University, Kunming 650500, People's Republic of China*
[74]*Zhejiang University, Hangzhou 310027, People's Republic of China*
[75]*Zhengzhou University, Zhengzhou 450001, People's Republic of China*

(Received 19 June 2022; accepted 28 July 2022; published 22 August 2022)

[a]Also at the Moscow Institute of Physics and Technology, Moscow 141700, Russia.
[b]Also at the Novosibirsk State University, Novosibirsk 630090, Russia.
[c]Also at the NRC "Kurchatov Institute", PNPI, 188300 Gatchina, Russia.
[d]Also at Goethe University Frankfurt, 60323 Frankfurt am Main, Germany.
[e]Also at Key Laboratory for Particle Physics, Astrophysics and Cosmology, Ministry of Education; Shanghai Key Laboratory for Particle Physics and Cosmology; Institute of Nuclear and Particle Physics, Shanghai 200240, People's Republic of China.
[f]Also at Key Laboratory of Nuclear Physics and Ion-beam Application (MOE) and Institute of Modern Physics, Fudan University, Shanghai 200443, People's Republic of China.
[g]Also at State Key Laboratory of Nuclear Physics and Technology, Peking University, Beijing 100871, People's Republic of China.
[h]Also at School of Physics and Electronics, Hunan University, Changsha 410082, China.
[i]Also at Guangdong Provincial Key Laboratory of Nuclear Science, Institute of Quantum Matter, South China Normal University, Guangzhou 510006, China.
[j]Also at Frontiers Science Center for Rare Isotopes, Lanzhou University, Lanzhou 730000, People's Republic of China.
[k]Also at Lanzhou Center for Theoretical Physics, Lanzhou University, Lanzhou 730000, People's Republic of China.
[l]Also at the Department of Mathematical Sciences, IBA, Karachi 75270, Pakistan.

Published by the American Physical Society under the terms of the Creative Commons Attribution 4.0 International license. Further distribution of this work must maintain attribution to the author(s) and the published article's title, journal citation, and DOI. Funded by SCOAP³.

The hadronic decay $\eta_c(2S) \to 3(\pi^+\pi^-)$ is observed with a statistical significance of 9.3 standard deviations using $(448.1 \pm 2.9) \times 10^6$ $\psi(3686)$ events collected by the BESIII detector at the BEPCII collider. The measured mass and width of $\eta_c(2S)$ are $(3643.4 \pm 2.3\,(\text{stat}) \pm 4.4\,(\text{syst}))$ MeV/c^2 and $(19.8 \pm 3.9\,(\text{stat}) \pm 3.1\,(\text{syst}))$ MeV, respectively, which are consistent with the world average values within two standard deviations. The product branching fraction $\mathcal{B}[\psi(3686) \to \gamma\eta_c(2S)] \times \mathcal{B}[\eta_c(2S) \to 3(\pi^+\pi^-)]$ is measured to be $(9.2 \pm 1.0\,(\text{stat}) \pm 1.2\,(\text{syst})) \times 10^{-6}$. Using $\mathcal{B}[\psi(3686) \to \gamma\eta_c(2S)] = (7.0^{+3.4}_{-2.5}) \times 10^{-4}$, we obtain $\mathcal{B}[\eta_c(2S) \to 3(\pi^+\pi^-)] = (1.31 \pm 0.15\,(\text{stat}) \pm 0.17\,(\text{syst})\,(^{+0.64}_{-0.47})\,(\text{extr})) \times 10^{-2}$, where the third uncertainty is from $\mathcal{B}[\psi(3686) \to \gamma\eta_c(2S)]$. We also measure the $\chi_{cJ} \to 3(\pi^+\pi^-)$ $(J = 0,\ 1,\ 2)$ decays via $\psi' \to \gamma\chi_{cJ}$ transitions. The branching fractions are $\mathcal{B}[\chi_{c0} \to 3(\pi^+\pi^-)] = (2.080 \pm 0.006\,(\text{stat}) \pm 0.068\,(\text{syst})) \times 10^{-2}$, $\mathcal{B}[\chi_{c1} \to 3(\pi^+\pi^-)] = (1.092 \pm 0.004\,(\text{stat}) \pm 0.035\,(\text{syst})) \times 10^{-2}$, and $\mathcal{B}[\chi_{c2} \to 3(\pi^+\pi^-)] = (1.565 \pm 0.005\,(\text{stat}) \pm 0.048\,(\text{syst})) \times 10^{-2}$.

DOI: 10.1103/PhysRevD.106.032014

I. INTRODUCTION

In recent years, remarkable experimental and theoretical progress has been made in charmonium studies. All predicted charmonium states below the open-charm threshold have been observed experimentally, and to a large extent, the measured spectra agree with the theoretical predictions based on quantum chromodynamics (QCD) [1–3] and QCD-inspired potential models [4–6]. However, there are still problems or puzzles that need to be understood.

It is predicted that the ratio of branching fractions of $\psi(3686)$ and J/ψ decaying into the same light hadron final states is around 12%, which was first proposed by Appelquist and Politzer using perturbative QCD [7]. This is valid in most of the measured hadronic channels [8], except for the decays into pseudoscalar vector pairs and vector tensor pairs, which are suppressed by at least an order of magnitude.

The $\eta_c(2S)$ and $\eta_c(1S)$ are the spin-singlet partners of ψ' $[\psi' \equiv \psi(3686)]$ and J/ψ, but two different ratios are calculated by the authors of Refs. [9,10], suggesting two possibilities:

$$\frac{\mathcal{B}[\eta_c(2S) \to \text{hadrons}]}{\mathcal{B}[\eta_c(1S) \to \text{hadrons}]} \simeq \frac{\mathcal{B}[\psi' \to \text{hadrons}]}{\mathcal{B}[J/\psi \to \text{hadrons}]} \simeq 12\%,$$

or

$$\frac{\mathcal{B}[\eta_c(2S) \to \text{hadrons}]}{\mathcal{B}[\eta_c(1S) \to \text{hadrons}]} \simeq 1,$$

respectively. Using information on light hadronic final states [11], the authors of Ref. [12] recently examined this branching fraction ratio in several decay modes and found that the experimental data are significantly different from both of the two theoretical predictions, e.g., $\frac{\mathcal{B}[\eta_c(2S) \to \bar{K}K\pi]}{\mathcal{B}[\eta_c(1S) \to \bar{K}K\pi]} = 0.27^{+0.10}_{-0.07}$ [12].

The $\eta_c(2S)$ is the first excited state of the pseudoscalar ground state $\eta_c(1S)$, lying just below the mass of its vector counterpart, ψ'. It was first observed by the Belle collaboration in B meson decay, $B^\pm \to K^\pm\eta_c(2S)$, in the exclusive decay $\eta_c(2S) \to K^0_S K^\pm\pi^\mp$ [13]. This state was hereafter confirmed by *BABAR* [14], CLEO [15], and Belle [16] in the two-photon fusion process $\gamma\gamma \to \eta_c(2S) \to \bar{K}K\pi$, and by *BABAR* [17] and Belle [18] in the double charmonium production process $e^+e^- \to J/\psi + c\bar{c}$. The magnetic dipole (M1) transition between ψ' and $\eta_c(2S)$ was first observed by BESIII, where $\eta_c(2S)$ was reconstructed with the $K\bar{K}\pi$ mode [19]. Currently, only seven decay modes of $\eta_c(2S)$ have been observed experimentally, of which the branching fractions of four have been measured with uncertainties larger than 50% [11]. The sum of the four decay modes is around 5% of the total width of $\eta_c(2S)$. Among the discovered decay modes of $\eta_c(1S)$, the decay rate of $\eta_c(1S) \to 3(\pi^+\pi^-)$ is relatively large, while the decay of $\eta_c(2S) \to 3(\pi^+\pi^-)$ has not yet been seen. CLEO searched for this mode in ψ' radiative decay but no signal was observed [20].

The hadronic decays $\chi_{cJ} \to 3(\pi^+\pi^-)$ $(J = 0, 1, 2)$ were successively measured by the MARK I collaboration in 1978 [21] and the BES collaboration in 1999 [22]. Since then, the results have not been updated. In this work, we update the measurement of $\chi_{cJ} \to 3(\pi^+\pi^-)$ with much higher statistics.

We present herein a study of the $\eta_c(2S) \to 3(\pi^+\pi^-)$ and $\chi_{cJ} \to 3(\pi^+\pi^-)$ in ψ' radiative transitions. The measurement is based on a data sample corresponding to an integrated luminosity of 668.55 pb^{-1} ($(448.1 \pm 2.9) \times 10^6$ ψ' events [23]) produced at the peak of the ψ' resonance and collected by the BESIII detector at the BEPCII collider. Additional datasets recorded at the c.m. energies of 3.581 and 3.670 GeV with integrated luminosities of 85.7 and 84.7 pb^{-1}, respectively, are used to determine the nonresonant continuum background contributions.

II. BESIII DETECTOR AND MONTE CARLO SIMULATION

The BESIII detector [24] records e^+e^- collisions provided by the BEPCII storage ring [25], which operates with a peak luminosity of $1 \times 10^{33}\,\mathrm{cm}^{-2}\,\mathrm{s}^{-1}$ in the center-of-mass (c.m.) energy range from 2.00 to 4.95 GeV. The cylindrical core of the BESIII detector covers 93% of the full solid angle and consists of a helium-based multilayer drift chamber (MDC), a plastic scintillator time-of-flight system (TOF), and a CsI(Tl) electromagnetic calorimeter (EMC), which are all enclosed in a superconducting solenoidal magnet providing a 1.0 T magnetic field. The solenoid is supported by an octagonal flux-return yoke with resistive plate counter muon identification modules interleaved with steel. The charged-particle momentum resolution at 1 GeV/c is 0.5%, and the dE/dx resolution is 6% for the electrons from Bhabha scattering at 1 GeV. The EMC measures photon energies with a resolution of 2.5% (5%) at 1 GeV in the barrel (end cap) region. The time resolution of the TOF barrel part is 68 ps, while that of the end cap part is 110 ps.

Simulated data samples produced with GEANT4-based [26] Monte Carlo (MC) software, which includes the geometric description of the BESIII detector and the detector response, are used to determine detection efficiencies and to estimate background contributions. The simulation models the beam energy spread and initial state radiation (ISR) in the e^+e^- annihilations with the generator KKMC [27]. The generic MC sample includes the production of the ψ' resonance, the ISR production of the J/ψ, and the continuum processes incorporated in KKMC [27]. The known decay modes are generated with EVTGEN [28] using branching fractions taken from the Particle Data Group [11], and the remaining unknown charmonium decays are modeled with LUNDCHARM [29]. Final state radiation (FSR) from charged final state particles is incorporated using PHOTOS [30]. The exclusive decays of $\psi' \to \gamma X$ are generated following the angular distribution of $(1 + \lambda\cos^2\theta)$, where X refers to $\eta_c(2S)$ or χ_{cJ}, θ is the polar angle of the radiative photon in the rest frame of ψ', and the value of λ is set to 1 for $\eta_c(2S)$ and to 1, $-1/3$, $1/13$ for $\chi_{cJ}(J = 0, 1, 2)$ [31], respectively. The $X \to 3(\pi^+\pi^-)$ decay is generated uniformly in phase space (PHSP). Additionally, two exclusive MC samples, $\psi' \to \pi^0 3(\pi^+\pi^-)$ and $\psi' \to (\gamma_{\mathrm{FSR}})3(\pi^+\pi^-)$, are generated according to PHSP to estimate background contamination.

III. EVENT SELECTION

We search for $\eta_c(2S)$ in the exclusive decay $\psi' \to \gamma\eta_c(2S)$ with $\eta_c(2S) \to 3(\pi^+\pi^-)$ in events containing at least one radiative photon and six charged tracks. Charged tracks detected in the MDC are required to be within a polar angle (θ) range of $|\cos\theta| < 0.93$, where θ is defined with respect to the symmetry axis of the MDC (z axis). For charged tracks, the distance of closest approach to the interaction point must be less than 10 cm along the z axis, and less than 1 cm in the transverse plane. Charged-particle identification (PID) is based on the combined information from the energy deposited in the MDC (dE/dx) and the flight time measured by the TOF, which are used to determine a variable $\chi^2_{\mathrm{PID}}(h)$ for each track, where h denotes the pion, kaon, or proton hypothesis.

Photon candidates are identified using isolated showers in the EMC. The deposited energy of each shower must be larger than 25 MeV in both the barrel region ($|\cos\theta| < 0.80$) and end cap region ($0.86 < |\cos\theta| < 0.92$). To suppress electronic noise and showers unrelated to the event, the difference between the EMC time and the event start time is required to be within (0, 700) ns.

Candidate events having exactly six charged tracks with net charge zero and at least one candidate photon are retained. To improve the mass resolution and suppress background, the total four-momentum of the charged tracks and the photon candidate is constrained to the initial ψ' four-momentum by a kinematic fit (4C fit). If there is more than one photon candidate, the one resulting in the minimum χ^2 from the 4C fit (χ^2_{4C}) is selected as the radiative photon. The background due to incorrect PID is suppressed by using $\chi^2_{\mathrm{tot}} = \chi^2_{\mathrm{4C}} + \sum_i \chi^2_{\mathrm{PID}}(\pi)$, where i runs over the six charged tracks. The candidate events satisfying $\chi^2_{\mathrm{tot}} < 200$ and $\chi^2_{\mathrm{4C}} < 44$ are kept as the $\gamma 3(\pi^+\pi^-)$ candidate events.

Background events from the $\psi' \to \pi^+\pi^- J/\psi$ process are removed by a J/ψ veto, which requires the recoil masses of all $\pi^+\pi^-$ pairs be below the J/ψ mass ($M^{\mathrm{rec}}_{\pi^+\pi^-} < 3.05\ \mathrm{GeV}/c^2$). Background events from $\psi' \to \eta X$ with $\eta \to \gamma\pi^+\pi^-$ are greatly suppressed by the η veto, which requires the invariant mass of $\gamma\pi^+\pi^-$ be outside the η signal region, $M_{\gamma\pi^+\pi^-} > 0.554$ or $M_{\gamma\pi^+\pi^-} < 0.538\ \mathrm{GeV}/c^2$.

The χ^2_{4C} and η mass window requirements are optimized by maximizing $S/\sqrt{S+B}$, where S and B are the numbers of expected $\eta_c(2S)$ signal and background events in the $\eta_c(2S)$ signal region in data, respectively. The $\eta_c(2S)$ signal region is defined as $(3.60, 3.66)\ \mathrm{GeV}/c^2$. S is calculated by $S = N^{\mathrm{tot}}_{\psi'}\mathcal{B}[\psi' \to \gamma\eta_c(2S)]\mathcal{B}[\eta_c(2S) \to 3(\pi^+\pi^-)]\epsilon$, where $N^{\mathrm{tot}}_{\psi'}$ is the number of ψ' events [23] and ϵ is the detection efficiency. Without using experimental information on $\mathcal{B}[\eta_c(2S) \to 3(\pi^+\pi^-)]$, we assume $\mathcal{B}[\eta_c(2S) \to 3(\pi^+\pi^-)]/\mathcal{B}[\eta_c(2S) \to K^0_S K^-\pi^+\pi^+\pi^-] = \mathcal{B}[\eta_c(1S) \to 3(\pi^+\pi^-)]/\mathcal{B}[\eta_c(1S) \to K^0_S K^-\pi^+\pi^+\pi^-]$. Here $\mathcal{B}[\eta_c(1S) \to 3(\pi^+\pi^-)]$, $\mathcal{B}[\eta_c(1S, 2S) \to K^0_S K^-\pi^+\pi^+\pi^-]$, and $\mathcal{B}[\psi' \to \gamma\eta_c(2S)]$ are taken from the world average values [11], and B is estimated with the generic MC sample.

IV. BACKGROUND ESTIMATION

The analysis of the generic MC sample for the ψ' decays with TopoAna [32] indicates that the dominant background

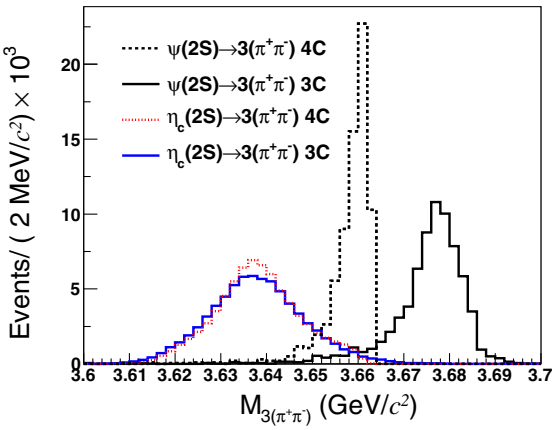

FIG. 1. Comparison between 3C and 4C kinematic fits (unnormalized). Shown in the plot are the invariant mass distributions of $3(\pi^+\pi^-)$ of signal events from the 3C fit (blue solid line) and 4C fit (red dashed line), those of background events of $\psi' \to 3(\pi^+\pi^-)$ from the 3C fit (black solid line) and 4C fit (black dashed line).

contributions come from two sources: (1) $\psi' \to 3(\pi^+\pi^-)$ with a fake photon or a photon from FSR in the final state; (2) $\psi' \to \pi^0 3(\pi^+\pi^-)$ with π^0 decaying into a $\gamma\gamma$ pair. The remaining background events are from hundreds of decay modes with small contributions to the signal processes, which distribute smoothly in the $3(\pi^+\pi^-)$ invariant mass spectrum. In the χ_{cJ} signal region from 3.35 to 3.58 GeV/c^2, the possible peaking background processes, $\chi_{cJ} \to K^0_S K 3\pi$, $K^+K^-2(\pi^+\pi^-)$, $K^0_S K^0_S \pi^+\pi^-$, and $\mu^+\mu^- 2(\pi^+\pi^-)$, are studied, and the contaminations from these processes are found to be negligible.

A. $\psi' \to 3(\pi^+\pi^-)$

The background from $\psi' \to 3(\pi^+\pi^-)$ with a fake photon satisfying the 4C fit contributes to a peak near the $\eta_c(2S)$ mass and decreases rapidly with higher mass in the $3(\pi^+\pi^-)$ mass spectrum due to the threshold of 25 MeV for a photon. The inclusion of a fake photon in the 4C kinematic fit shifts the $3(\pi^+\pi^-)$ invariant mass peak lower compared to the true mass. This shift can be corrected by performing a modified kinematic fit in which the energy of the measured photon is allowed to vary in the fit (3C fit). The $\eta_c(2S)$ mass resolution from the 3C fit is similar to that from the 4C fit, while the former can separate the background events from the $\eta_c(2S)$ signal significantly (see Fig. 1). Therefore, the invariant mass spectrum from the 3C fit, $M^{\rm 3C}_{3(\pi^+\pi^-)}$, is used to determine the signal yield.

The background events from the $\psi' \to 3(\pi^+\pi^-)$ process with an FSR photon have the same final state as the signal process and can contaminate the $\eta_c(2S)$ signal due to a long tail from 3.60 to 3.66 GeV/c^2 in the $M^{\rm 3C}_{3(\pi^+\pi^-)}$ distribution. The size of the tail depends on the FSR fraction, which is defined as $R_{\rm FSR} = N_{\rm FSR}/N_{\rm nonFSR}$, where $N_{\rm FSR}$ ($N_{\rm nonFSR}$) is the number of events with (without) an FSR photon surviving the selection. The difference in the FSR fraction between data and MC simulation is studied by using a control sample $\psi' \to \gamma\chi_{c0}, \chi_{c0} \to (\gamma_{\rm FSR})3(\pi^+\pi^-)$ and subsequently corrected for by the FSR correction factor.

The FSR photon in the control sample is required to be reconstructed. The event selection criteria of the control sample are similar to those of the signal sample, except that the final states contain two photons. The softer photon is treated as the FSR photon, and in the 3C fit, the energy of the FSR photon is free. The process $\psi' \to \pi^0 3(\pi^+\pi^-)$ is a dominant background contribution to the control sample, since it has the same final state particles as the control sample. The candidate events satisfying $0.115 < M_{\gamma\gamma} < 0.150$ GeV/c^2 are rejected to remove the background events from $\psi' \to \pi^0 3(\pi^+\pi^-)$, where $M_{\gamma\gamma}$ is the invariant mass of $\gamma\gamma$. The requirement of $E_{\rm hard} < 0.2$ GeV is placed to remove the background events from $\psi' \to \gamma\chi_{c1,2}, \chi_{c1,2} \to (\gamma_{\rm FSR})3(\pi^+\pi^-)$, where $E_{\rm hard}$ is the energy of the harder photon. For this sample, $R^{\rm Data}_{\rm FSR}$ is determined by fitting the $M^{\rm 3C}_{3(\pi^+\pi^-)}$ spectrum. The FSR and nonFSR events are described by the corresponding MC shapes determined from the $\psi' \to (\gamma_{\rm FSR})3(\pi^+\pi^-)$ MC simulation and convolved with a Gaussian function to account for the resolution difference between data and MC simulation. The parameters of the Gaussian function are free in the fit. The background events from $\psi' \to \pi^0 3(\pi^+\pi^-)$ and $\psi' \to \gamma\chi_{c1,2}, \chi_{c1,2} \to (\gamma_{\rm FSR})3(\pi^+\pi^-)$ are dominant, and their shapes are determined directly from the MC simulated events surviving the $\gamma\gamma 3(\pi^+\pi^-)$ selection. The distribution of the remaining background events is smooth and thus modeled by an ARGUS function [33]. The number of events of each component is a free parameter, and the fit result is shown in Fig. 2. From the fit, we obtain $R^{\rm Data}_{\rm FSR} = 0.70 \pm 0.05$. From the MC simulation, we obtain $R^{\rm MC}_{\rm FSR} = 0.43$. The FSR correction factor is defined as $f_{\rm FSR} = R^{\rm Data}_{\rm FSR}/R^{\rm MC}_{\rm FSR} = 1.62 \pm 0.13$, where the uncertainty is statistical.

Though emitting an FSR photon changes the charge conjugate parity of the $3(\pi^+\pi^-)$ system, the fact that the $f_{\rm FSR}$ only accounts for the difference on FSR fraction between data and MC simulation and the FSR fraction in MC simulation depends on the masses of the mother and daughter particles [30] proves the independence of the $f_{\rm FSR}$ on the charge conjugate parity of the system. Thus, the $f_{\rm FSR}$ obtained from χ_{c0} decay is applied for ψ' decay in this work. In the fit to determine the numbers of $\eta_c(2S)$ and χ_{cJ} signal events, the background shape from $\psi' \to (\gamma_{\rm FSR})3(\pi^+\pi^-)$ is described by the sum of MC simulated shapes $\psi' \to 3(\pi^+\pi^-)$ and $\psi' \to \gamma_{\rm FSR} 3(\pi^+\pi^-)$ with the FSR fraction corrected by $f_{\rm FSR}$.

B. $\psi' \to \pi^0 3(\pi^+\pi^-)$

The background from $\psi' \to \pi^0 3(\pi^+\pi^-)$ is measured from data by reconstructing the $\gamma\gamma 3(\pi^+\pi^-)$ events, where

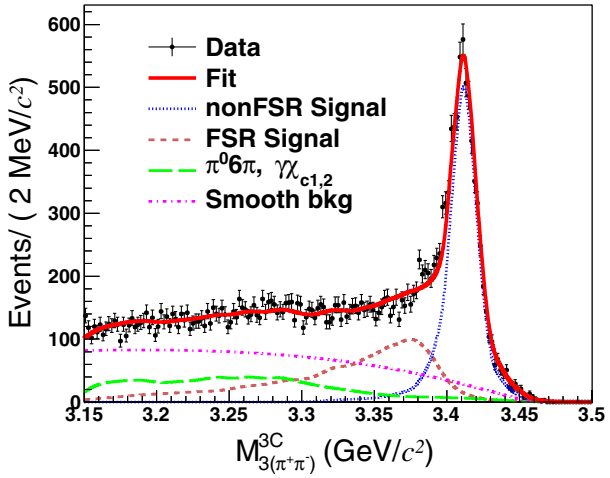

FIG. 2. Fitted distribution of $M^{3C}_{3(\pi^+\pi^-)}$ from $\psi' \to \gamma\chi_{c0}$, $\chi_{c0} \to (\gamma_{\rm FSR})3(\pi^+\pi^-)$ events. The black dots with error bars are the data, the red solid line is the best fit result, the blue dotted line represents the nonFSR component, the brown dashed line represents the FSR component, the green long-dashed line shows the contribution from known background components, and the pink dash-dotted line represents the smooth shape used to describe the remaining background events.

the $\gamma\gamma$ pair forms a π^0 candidate. In the case of more than two photons, the π^0 candidate with the minimum χ^2 from a 5C kinematic fit (4C fit plus a π^0 mass constraint) is selected. The background contribution is suppressed with the requirement $\chi^2_{\rm 5C} < 50$. The other selection criteria are the same as in the signal selection. Imposing the signal selection, the background shape of $\psi' \to \pi^0 3(\pi^+\pi^-)$ is estimated via

$$\left(\frac{dN}{dM_{3(\pi^+\pi^-)}}\right)^{\rm 3C} = \left(\frac{dN}{dM_{3(\pi^+\pi^-)}}\right)^{\rm 5C} \times \frac{\epsilon^{\rm 3C}_{\gamma 3(\pi^+\pi^-)}}{\epsilon^{\rm 5C}_{\pi^0 3(\pi^+\pi^-)}},$$

where $M^{\rm 5C}_{3(\pi^+\pi^-)}$ is the invariant mass distribution of $3(\pi^+\pi^-)$ from the 5C fit for the events from data passing the $\pi^0 3(\pi^+\pi^-)$ selection, and $\epsilon^{\rm 3C}_{\gamma 3(\pi^+\pi^-)}$ and $\epsilon^{\rm 5C}_{\pi^0 3(\pi^+\pi^-)}$ are the efficiencies as functions of the $3(\pi^+\pi^-)$ mass with which the $\psi' \to \pi^0 3(\pi^+\pi^-)$ MC simulated events pass the $\gamma 3(\pi^+\pi^-)$ and $\pi^0 3(\pi^+\pi^-)$ selections, respectively.

C. Continuum contribution

The background contribution from the continuum processes (including the initial state radiation) is estimated using the datasets taken at the c.m. energies ($E_{\rm c.m.}$) of 3.581 and 3.670 GeV. The momenta and energies of final state particles are scaled to account for the difference in c.m. energy. The mass spectrum is normalized based on the differences in the integrated luminosity and cross section. The energy dependence of the cross section is measured by the *BABAR* experiment [34], and we determine it

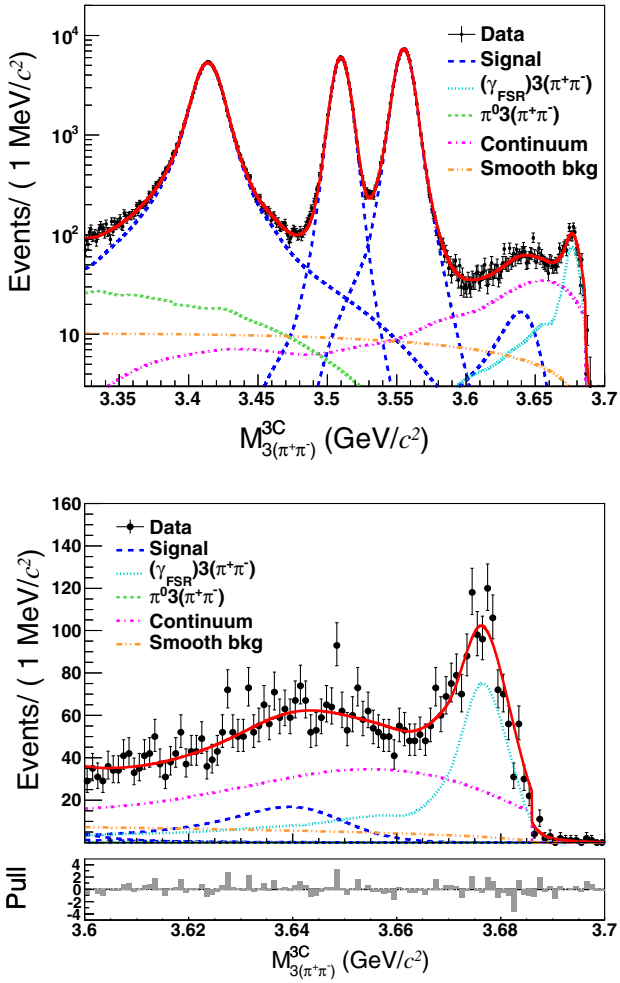

FIG. 3. Invariant mass distributions of $3(\pi^+\pi^-)$ after a 3C fit in the whole fit range (top) and in the range only containing $\eta_c(2S)$ signal (bottom). Dots with error bars are data, the red solid curve is the best fit result, the blue long-dashed lines show the $\eta_c(2S)$ and χ_{cJ} signal shapes, the cyan dotted line represents the contribution from $\psi' \to (\gamma_{\rm FSR})3(\pi^+\pi^-)$, the green dashed line shows the contribution from $\psi' \to \pi^0 3(\pi^+\pi^-)$, the pink dash-dotted line is the continuum contribution, and the orange dash-dot-dotted line represents the smooth background.

to be proportional to $1/s^{2.21\pm0.67}$ ($s = E^2_{\rm c.m.}$) by a fit to the measured cross sections of $e^+e^- \to 3(\pi^+\pi^-)$, where the uncertainty includes the statistical and systematic uncertainties.

V. SIGNAL DETERMINATION

The signal yields are determined by a fit to the $M^{\rm 3C}_{3(\pi^+\pi^-)}$ spectrum using an unbinned maximum likelihood method, as shown in Fig. 3. The fit range is from 3.325 to 3.700 GeV/c^2, which includes the χ_{cJ} signals. The line shape of $\eta_c(2S)$ is described by

$$[E^3_\gamma \times BW(m) \times f_d(E_\gamma) \times \epsilon(m)] \otimes G(\delta m, \sigma),$$

TABLE I. Signal yields, corrected signal efficiencies, and branching fractions for $\eta_c(2S)$ and χ_{cJ} decays. The branching fractions of $\chi_{cJ} \to 3(\pi^+\pi^-)$ from the world average values [11] are also shown.

Channel	$N^{\rm sig}_{\rm data}$	$\epsilon^{\rm corr}$ (%)	$\mathcal{B}_{\rm measured}$ ($\times 10^{-2}$)	$\mathcal{B}_{\rm PDG}$ ($\times 10^{-2}$)
$\eta_c(2S) \to 3(\pi^+\pi^-)$	568.8 ± 63.3	13.84 ± 0.01	$1.31 \pm 0.15 \pm 0.17^{+0.64}_{-0.47}$	$\cdots$
$\chi_{c0} \to 3(\pi^+\pi^-)$	145300 ± 396	15.92 ± 0.01	$2.080 \pm 0.006 \pm 0.068$	1.20 ± 0.18
$\chi_{c1} \to 3(\pi^+\pi^-)$	84317 ± 299	17.67 ± 0.01	$1.092 \pm 0.004 \pm 0.035$	0.54 ± 0.14
$\chi_{c2} \to 3(\pi^+\pi^-)$	112510 ± 347	16.85 ± 0.01	$1.565 \pm 0.005 \pm 0.048$	0.84 ± 0.18

where m is the mass of $3(\pi^+\pi^-)$, E_γ is the energy of the transition photon in the rest frame of ψ', $BW(m)$ is the Breit-Wigner function, $f_d(E_\gamma)$ is a function to damp the diverging tail from E_γ^3, $\epsilon(m)$ is the efficiency curve as a function of m, and $G(\delta m, \sigma)$ is a Gaussian function describing the detector resolution determined from MC simulation. The $f_d(E_\gamma)$ form proposed by the KEDR collaboration [35], $E_0^2/[E_\gamma E_0 + (E_\gamma - E_0)^2]$, is used in the nominal fit, where E_0 is the most probable energy of the transition photon. The efficiency curve is parametrized by $(m/{\rm GeV}/c^2)(1-(m/3.6747\,{\rm GeV}/c^2)^2)^{0.303} \times e^{-3.75(1-(m/3.6747\,{\rm GeV}/c^2)^2)}$, obtained by fitting the efficiencies determined at each m using an ARGUS function [33]. The χ_{cJ} line shapes are obtained directly from the MC simulations. The $\eta_c(2S)$ and χ_{cJ} line shapes are convolved with additional Gaussian functions to account for the mass resolution difference between data and MC simulations. For χ_{cJ}, the parameters of the Gaussian function are determined in the fit, while for $\eta_c(2S)$ they are fixed to the values extrapolated from the χ_{cJ} results assuming a linear relationship. The background shapes have been estimated as described above. For $\psi' \to \pi^0 3(\pi^+\pi^-)$ and the continuum contributions, the shapes and the numbers of events are fixed. For $\psi' \to (\gamma_{\rm FSR})3(\pi^+\pi^-)$, the shape is from MC simulation convolved with a Gaussian function with floating parameters and the number of events is left free. In MC simulation, the fraction of FSR events is corrected by $f_{\rm FSR}$. The remaining background distribution is smooth, thus is described by an ARGUS function with the number of events a free parameter in the fit. It is assumed there is no interference between the signal and the continuum events. With toy MC samples, we validate that the output values of the mass and width of the $\eta_c(2S)$ signal, as well as the numbers of $\eta_c(2S)$ and χ_{cJ} signal events, are consistent with the inputs within one standard deviation, suggesting that the fit procedure has no bias.

The signal yields ($N^{\rm sig}_{\rm data}$) obtained from the fit are summarized in Table I. The χ^2/ndf value of the fit is $557.2/359 = 1.51$, where ndf is the number of degrees of freedom. The statistical significance of $\eta_c(2S)$ is calculated to be 10.8σ from the difference of the logarithmic likelihoods [36], $-2\ln(\mathcal{L}_0/\mathcal{L}_{\rm max})$, where $\mathcal{L}_{\rm max}$ and $\mathcal{L}_0$ are the maximized likelihoods with and without the signal component, respectively. The difference in the number of degrees of freedom ($\Delta{\rm ndf} = 3$) has been taken into account. The largest systematic uncertainty, as described in Sec. VI, is from the fit to the mass spectrum. Alternative fits to the $M^{\rm 3C}_{3(\pi^+\pi^-)}$ spectrum under different fit conditions are performed, and the $\eta_c(2S)$ signal significance is larger than 9.3σ in all cases. We measure the mass and width of $\eta_c(2S)$, which are $M = (3643.4 \pm 2.3 \pm 4.4)$ MeV/c^2 and $\Gamma = (19.8 \pm 3.9 \pm 3.1)$ MeV, respectively. The branching fraction is calculated using

$$\mathcal{B}[X \to 3(\pi^+\pi^-)] = \frac{N^{\rm sig}_{\rm data}}{N^{\rm tot}_{\psi'} \times \mathcal{B}(\psi' \to \gamma X) \times \epsilon_{\rm corr}},$$

where X refers to $\eta_c(2S)$ or χ_{cJ}, $\mathcal{B}(\psi' \to \gamma X)$ is the branching fraction of $\psi' \to \gamma X$ [11], and $\epsilon_{\rm corr} = \epsilon_{\rm MC} * f_{\rm corr}$ is the corrected signal detection efficiency. The correction factor of the efficiency takes into account small differences between data and simulation in the single-track reconstruction efficiency; it is $f_{\rm corr} = [\sum_{\rm i}^{N_{\rm sel}} \prod_{\rm j}^{6} w_{ij}(p_t, \cos\theta)]/N_{\rm sel}$, where $N_{\rm sel}$ is the number of signal MC simulated PHSP events surviving the event selection, i and j run over the surviving events and the six charged tracks, respectively, w_{ij} is the charged track reconstruction weight factor in bins of $(p_t, \cos\theta)$, and p_t is the transverse momentum of the track. The values of w_{ij} are obtained using the control sample $J/\psi \to \pi^+\pi^-\pi^0$. $f_{\rm corr}$ is calculated using a sampling method, where w_{ij} is sampled according to $G(w_{ij}, \Delta w_{ij})$. Here Δw_{ij} is the uncertainty of w_{ij}, G is a Gaussian function. Using 10000 samples, the resulting $f_{\rm corr}$ follows a Gaussian distribution. The mean value of the Gaussian distribution is taken as the nominal efficiency correction factor, and the standard deviation is taken as the uncertainty, labeled as $\Delta f_{\rm corr}$. Table I lists the corrected efficiencies and calculated branching fractions, where the first uncertainty is statistical, the second systematic, and the third from the uncertainty of $\mathcal{B}[\psi' \to \gamma\eta_c(2S)]$.

Our measurement indicates that the branching fractions for $\chi_{cJ} \to 3(\pi^+\pi^-)$ are about twice as large as the current world average. To validate our results, we perform a number of cross-checks. We divide the dataset into two sub-datasets, collected in 2009 and 2012, respectively, and compare the branching fractions of $\chi_{cJ} \to 3(\pi^+\pi^-)$

TABLE II. Relative systematic uncertainties in the measurements of the branching fractions (in %), where $f = 3(\pi^+\pi^-)$, and absolute systematic uncertainties in the $\eta_c(2S)$ mass (MeV/c^2) and width (MeV) measurements. For the $\eta_c(2S) \to 3(\pi^+\pi^-)$ mode, the value in parentheses is the total systematic uncertainty without including the uncertainty from $\mathcal{B}(\psi' \to \gamma\eta_c(2S))$ [12].

Sources	$\mathcal{B}(\eta_c(2S) \to f)$	$\mathcal{B}(\chi_{c0} \to f)$	$\mathcal{B}(\chi_{c1} \to f)$	$\mathcal{B}(\chi_{c2} \to f)$	Mass	Width
Efficiency correction factor	0.07	0.06	0.06	0.06	···	···
Photon reconstruction	1.00	1.00	1.00	1.00	···	···
Kinematic fit	0.70	0.53	0.53	0.74	···	···
J/ψ veto	2.36	0.81	0.92	1.01	0.90	1.08
η veto	1.55	0.50	0.62	0.74	0.60	0.48
Damping function form	1.20	0.10	0.05	0.00	1.80	1.19
Efficiency curve	0.63	0.08	0.01	0.10	0.80	0.88
Gaussian resolutions	3.36	0.01	0.01	0.01	1.34	0.66
Size of FSR correction factor	2.23	0.05	0.01	0.01	0.20	0.28
Number of $\psi' \to \pi^0 3(\pi^+\pi^-)$ events	0.12	0.07	0.01	0.01	1.40	0.09
Shape of $\psi' \to \pi^0 3(\pi^+\pi^-)$	0.07	0.18	0.01	0.01	0.60	0.04
Number of continuum events	7.04	0.12	0.09	0.05	1.34	1.82
Shape of continuum	4.52	0.04	0.01	0.02	2.40	0.95
MC simulation	1.43	1.88	1.16	1.13	···	···
Possible interference	8.61	···	···	···	1.60	1.05
Number of ψ' events	0.60	0.60	0.60	0.60	···	···
Branching fraction	$^{+48.57}_{-35.71}$	2.04	2.46	2.10	···	···
MC statistics	0.34	0.58	0.54	0.56	···	···
Total	$^{+50.33}_{-38.07}$ (13.20)	3.26	3.25	3.08	4.40	3.07

obtained from the two sub-datasets. The results are consistent with each other and agree with the nominal results. Additionally, two individual studies of measurements of branching fractions of $\chi_{cJ} \to 3(\pi^+\pi^-)$ are performed and the results from two cross-checks agree well with the reported results.

VI. SYSTEMATIC UNCERTAINTIES

Table II summarizes the sources of systematic uncertainties in measuring the branching fractions and the parameters of $\eta_c(2S)$. They are described in the following.

The systematic uncertainty from the efficiency correction factor is given by $\Delta f_{\rm corr}/f_{\rm corr}$.

Based on the study of the photon detection efficiency using the control samples of $J/\psi \to \rho^0\pi^0$ and $e^+e^- \to \gamma\gamma$ [37], the systematic uncertainty due to photon reconstruction is 1% per photon.

In the kinematic fit, the helix parameters of charged tracks in MC simulation have been corrected to improve the consistency between data and simulation [38]. The systematic uncertainty from the kinematic fit is taken as half of the difference between the efficiencies with and without track helix parameter correction.

To estimate the uncertainty from the J/ψ veto, we vary the maximum requirement on $M^{\rm rec}_{\pi^+\pi^-}$ from 3.00 to 3.08 GeV/c^2 in steps of 0.01 GeV/c^2. The maximum difference of the results with respect to the nominal one is taken as the systematic uncertainty from the J/ψ veto. To estimate the uncertainty from the η veto, the mass window of the η veto is changed to be (0.538, 0.552), (0.536, 0.554), (0.534, 0.556), (0.532, 0.558), (0.530, 0.560), (0.528, 0.562), or $(0.526, 0.564)$ GeV/c^2. The results under the different windows are obtained, and the maximum difference with the nominal one is taken as the systematic uncertainty from the η veto.

An alternative damping function used by the CLEO collaboration [39], $f_d(E_\gamma) = \exp(-E_\gamma^2/8\beta^2)$, is chosen to estimate the uncertainty from the damping function, where β is a free parameter. The difference between the two damping functions is taken as the systematic uncertainty. We model the efficiency curve using a threshold function with the parametrized form of $\sqrt[4]{3.675-(m/{\rm GeV}/c^2)}[1.5-1.5(3.675-(m/({\rm GeV}/c^2))]$, and take the difference between the two functions as the systematic uncertainty. The resolutions of two Gaussian functions for the line shape of the $\eta_c(2S)$ signal are varied by $\pm1\sigma$, and the largest difference is taken as the systematic uncertainty.

The systematic uncertainties related to the background contributions are from the FSR process, continuum, and $\psi' \to \pi^0 3(\pi^+\pi^-)$, of which the first two may influence our fit results in the $\eta_c(2S)$ mass region. We vary the FSR correction factor by $\pm1\sigma$ and take the largest difference as

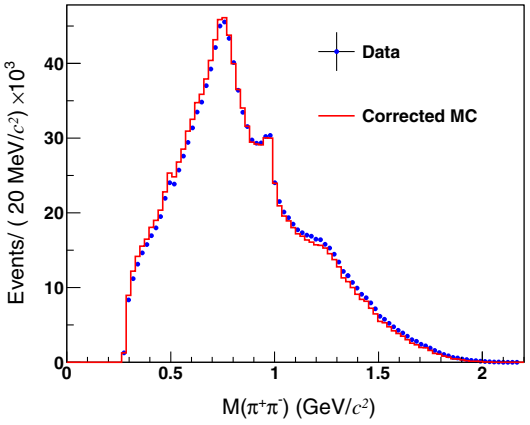

FIG. 4. Invariant mass distributions of $\pi^+\pi^-$ from data and the corrected MC simulation. The blue dots represent the data and the red solid line stands for the corrected MC simulation.

the uncertainty from the shape of the FSR process. The number of continuum events is determined by the normalization factor calculated using the integrated luminosity and cross section, where the latter is proportional to $1/s^{2.21\pm0.67}$. Taking into account a 1.0% uncertainty of the integrated luminosity, a new normalization factor is calculated, and the mass spectrum is fitted with the new fixed number of continuum events. The differences of the measured results with respect to the nominal ones are taken as the uncertainty from the luminosity. Additionally, we change the cross section by varying the exponent by ±0.67 and refit the mass spectrum. The uncertainty from the cross section is estimated to be the difference of the measured result. Finally, the systematic uncertainty from the number of continuum events is determined by adding the uncertainties from the luminosity and the cross section in quadrature. We modify the number of the background events of $\psi' \to \pi^0 3(\pi^+\pi^-)$ by $\pm1\sigma$ to estimate the uncertainty from the number of $\psi' \to \pi^0 3(\pi^+\pi^-)$ events. The line shapes of continuum and $\psi' \to \pi^0 3(\pi^+\pi^-)$ background are smoothed by rookeyspdf [40] in the nominal fit. We use roohistpdf [41] and take the difference under the two methods as the systematic uncertainty.

There are obvious ρ and $f_0(980)$ intermediate states in the $M_{\pi^+\pi^-}$ distribution from the data, as shown in Fig. 4, while these states are not taken into account in the PHSP MC simulation. We correct the $M_{\pi^+\pi^-}$ distribution from PHSP MC simulation to agree with data, as shown by the red line in Fig. 4. Additionally, the distributions of track momenta disagree between data and MC simulation, and we correct the MC sample similarly. The difference in detection efficiency with and without these corrections is taken as the systematic uncertainty. The uncertainty of assuming $\psi' \to \gamma\chi_{cJ}$ as a pure electric dipole transition is studied by considering the contribution from higher-order multipole amplitudes [42–44] in the MC simulation, and the differences of the efficiency, 1.0% for χ_{c1} and 0.2% for χ_{c2}, are taken as the systematic uncertainties. As a conservative estimate, we assign a 1.0% uncertainty for assuming $\psi' \to \gamma\eta_c(2S)$ as a pure magnetic dipole transition due to the absence of experimental measurements of higher-order multipole amplitudes. The systematic uncertainty from the MC simulation is calculated by adding above uncertainties in quadrature.

There could be interference between the signal process and the $e^+e^- \to \gamma 3(\pi^+\pi^-)$ process when the quantum numbers of the two systems are the same. To estimate the uncertainty of the assumption of no interference in the nominal fit, we include the contribution from possible interferences into the mass spectrum fit and take the maximum differences of the measured branching fractions and the measured mass and width of $\eta_c(2S)$ relative to the nominal ones as the uncertainty. Using the difference of the maximum likelihoods and the number of degrees of freedom with and without the interference effect, the significance of the interference contribution is calculated to be 0.54σ.

The number of ψ' events is determined to be $(448.1 \pm 2.9) \times 10^6$ [23]; therefore 0.6% is taken as the uncertainty. The systematic uncertainties from branching fractions of $\psi' \to \gamma X$ are taken from the world average values [11], where X is $\eta_c(2S)$ or χ_{cJ}. The uncertainty from the statistics of the signal MC sample is considered as well.

VII. CONCLUSION

Using $(448.1 \pm 2.9) \times 10^6$ ψ' events collected by the BESIII detector, the hadronic decay $\eta_c(2S) \to 3(\pi^+\pi^-)$ is observed for the first time with a significance of 9.3σ.

The measured mass of $\eta_c(2S)$ is $(3643.4 \pm 2.3 \pm 4.4)$ MeV/c^2, and the width is $(19.8 \pm 3.9 \pm 3.1)$ MeV, which are consistent with the world average values within 2σ [11]. The product branching fraction $\mathcal{B}[\psi' \to \gamma\eta_c(2S)] \times \mathcal{B}[\eta_c(2S) \to 3(\pi^+\pi^-)]$ is measured to be $(9.2 \pm 1.0 \pm 1.2) \times 10^{-6}$. Using $\mathcal{B}[\psi' \to \gamma\eta_c(2S)] = (7.0^{+3.4}_{-2.5}) \times 10^{-4}$ [12], we obtain $\mathcal{B}[\eta_c(2S) \to 3(\pi^+\pi^-)] = (1.31 \pm 0.15 \pm 0.17^{+0.64}_{-0.47}) \times 10^{-2}$, where the first uncertainty is statistical, the second systematic, and the third from $\mathcal{B}[\psi' \to \gamma\eta_c(2S)]$.

Using $\mathcal{B}[\eta_c(1S) \to 3(\pi^+\pi^-)] = (1.7 \pm 0.4)\%$ [11], we calculate the ratio of branching fractions,

$$\frac{\mathcal{B}[\eta_c(2S) \to 3(\pi^+\pi^-)]}{\mathcal{B}[\eta_c(1S) \to 3(\pi^+\pi^-)]} = 0.77 \pm 0.59,$$

where the uncertainty is obtained by assuming the systematic uncertainties of both branching fractions are uncorrelated. This central value seems to lean slightly towards the prediction from Ref. [10] over the prediction from Ref. [9], but our result is compatible with both predictions.

We update the branching fractions of $\chi_{cJ} \to 3(\pi^+\pi^-)$, which are summarized in Table I. Compared to the world

average values [11], our measured values are almost twice as large.

ACKNOWLEDGMENTS

The BESIII collaboration thanks the staff of BEPCII and the IHEP computing center for their strong support. This work is supported in part by National Key R&D Program of China under Contracts No. 2020YFA0406300 and No. 2020YFA0406400; National Natural Science Foundation of China (NSFC) under Contracts No. 11635010, No. 11735014, No. 11835012, No. 11935015, No. 11935016, No. 11935018, No. 11961141012, No. 12022510, No. 12025502, No. 12035009, No. 12035013, No. 12192260, No. 12192261, No. 12192262, No. 12192263, No. 12192264, and No. 12192265; the Chinese Academy of Sciences (CAS) Large-Scale Scientific Facility Program; Joint Large-Scale Scientific Facility Funds of the NSFC and CAS under Contracts No. U1832207 and No. U2032108; CAS Key Research Program of Frontier Sciences under Contract No. QYZDJ-SSW-SLH040; 100 Talents Program of CAS; The Institute of Nuclear and Particle Physics (INPAC) and Shanghai Key Laboratory for Particle Physics and Cosmology; ERC under Contract No. 758462; European Union's Horizon 2020 research and innovation program under Marie Sklodowska-Curie Grant Agreement under Contract No. 894790; German Research Foundation DFG under Contract No. 443159800, Collaborative Research Center CRC 1044, GRK 2149, FOR 2359; Istituto Nazionale di Fisica Nucleare, Italy; Ministry of Development of Turkey under Contract No. DPT2006K-120470; National Science and Technology fund; National Science Research and Innovation Fund (NSRF) via the Program Management Unit for Human Resources & Institutional Development, Research and Innovation under Contract No. B16F640076; STFC (United Kingdom); Suranaree University of Technology (SUT), Thailand Science Research and Innovation (TSRI), and National Science Research and Innovation Fund (NSRF) under Contract No. 160355; The Royal Society, UK under Contracts No. DH140054 and No. DH160214; The Swedish Research Council; U.S. Department of Energy under Contract No. DE-FG02-05ER41374.

[1] N. Brambilla, A. Pineda, J. Soto, and A. Vairo, Rev. Mod. Phys. **77**, 1423 (2005).
[2] N. Brambilla *et al.*, Eur. Phys. J. C **71**, 1534 (2011).
[3] N. Brambilla *et al.*, Eur. Phys. J. C **74**, 2981 (2014).
[4] E. Eichten, K. Gottfried, T. Kinoshita, K. D. Lane, and T. M. Yan, Phys. Rev. D **17**, 3090 (1978).
[5] S. Godfrey and N. Isgur, Phys. Rev. D **32**, 189 (1985).
[6] T. Barnes, S. Godfrey, and E. S. Swanson, Phys. Rev. D **72**, 054026 (2005).
[7] T. Appelquist and H. D. Politzer, Phys. Rev. Lett. **34**, 43 (1975).
[8] S. J. Brodsky, G. P. Lepage, and S. F. Tuan, Phys. Rev. Lett. **59**, 621 (1987).
[9] M. Anselmino, M. Genovese, and E. Predazzi, Phys. Rev. D **44**, 1597 (1991).
[10] K. T. Chao, Y. F. Gu, and S. F. Tuan, Commun. Theor. Phys. **25**, 471 (1996).
[11] P. A. Zyla *et al.* (Particle Data Group), Prog. Theor. Exp. Phys. **2020**, 083C01 (2020), and 2021 update.
[12] H. P. Wang and C. Z. Yuan, Chin. Phys. C **46**, 071001 (2022).
[13] S. K. Choi *et al.* (Belle Collaboration), Phys. Rev. Lett. **89**, 102001 (2002).
[14] B. Aubert *et al.* (*BABAR* Collaboration), Phys. Rev. Lett. **92**, 142002 (2004).
[15] D. M. Asner *et al.* (CLEO Collaboration), Phys. Rev. Lett. **92**, 142001 (2004).
[16] H. Nakazawa *et al.* (Belle Collaboration), Nucl. Phys. B, Proc. Suppl. **184**, 220 (2008).
[17] B. Aubert *et al.* (*BABAR* Collaboration), Phys. Rev. D **72**, 031101 (2005).
[18] K. Abe *et al.* (Belle Collaboration), Phys. Rev. Lett. **98**, 082001 (2007).
[19] M. Ablikim *et al.* (BESIII Collaboration), Phys. Rev. Lett. **109**, 042003 (2012).
[20] D. C. Hennessy *et al.* (CLEO Collaboration), Phys. Rev. D **81**, 052002 (2010).
[21] W. Tanenbaum *et al.*, Phys. Rev. D **17**, 1731 (1978).
[22] J. Z. Bai *et al.* (BES Collaboration), Phys. Rev. D **60**, 072001 (1999).
[23] M. Ablikim *et al.* (BESIII Collaboration), Chin. Phys. C **42**, 023001 (2018).
[24] M. Ablikim *et al.* (BESIII Collaboration), Nucl. Instrum. Methods Phys. Res., Sect. A **614**, 345 (2010).
[25] C. H. Yu *et al.*, *Proceedings of IPAC2016, Busan, Korea, 2016* (JACoW, Geneva, Switzerland, 2016), 10.18429/JACoW-IPAC2016-TUYA01.
[26] S. Agostinelli *et al.* (Geant4 Collaboration), Nucl. Instrum. Methods Phys. Res., Sect. A **506**, 250 (2003).
[27] S. Jadach, B. F. L. Ward, and Z. Was, Comput. Phys. Commun. **130**, 260 (2000); Phys. Rev. D **63**, 113009 (2001).
[28] D. J. Lange, Nucl. Instrum. Methods Phys. Res., Sect. A **462**, 152 (2001); R. G. Ping, Chin. Phys. C **32**, 599 (2008).
[29] J. C. Chen, G. S. Huang, X. R. Qi, D. H. Zhang, and Y. S. Zhu, Phys. Rev. D **62**, 034003 (2000); R. L. Yang, R. G. Ping, and H. Chen, Chin. Phys. Lett. **31**, 061301 (2014).
[30] E. R. Was, Phys. Lett. B **303**, 163 (1993).

[31] W. M. Tanenbaum *et al.*, Phys. Rev. D **17**, 1731 (1978).
[32] X. Y. Zhou, S. X. Du, G. Li, and C. P. Shen, Comput. Phys. Commun. **258**, 107540 (2021).
[33] H. Albrecht *et al.* (ARGUS Collaboration), Phys. Lett. B **241**, 278 (1990).
[34] B. Aubert *et al.* (*BABAR* Collaboration), Phys. Rev. D **73**, 052003 (2006).
[35] V. V. Anashin *et al.*, Int. J. Mod. Phys. Conf. Ser. **02**, 188 (2011).
[36] S. S. Wilks, Ann. Math. Stat. **9**, 60 (1938).
[37] M. Ablikim *et al.* (BESIII Collaboration), Phys. Rev. D **81**, 052005 (2010).
[38] M. Ablikim *et al.* (BESIII Collaboration), Phys. Rev. D **87**, 012002 (2013).
[39] R. E. Mitchell *et al.* (CLEO Collaboration), Phys. Rev. Lett. **102**, 011801 (2009).
[40] K. S. Cranmer, Comput. Phys. Commun. **136**, 198 (2001).
[41] I. Antcheva *et al.*, Comput. Phys. Commun. **180**, 2499 (2009).
[42] M. Ablikim *et al.* (BESIII Collaboration), Phys. Rev. D **95**, 072004 (2017).
[43] G. Karl, S. Meshkov, and J. L. Rosner, Phys. Rev. Lett. **45**, 215 (1980).
[44] P. Moxhay and J. L. Rosner, Phys. Rev. D **28**, 1132 (1983).